RESEARCH PAPER



Synthesis, characterization and ab initio study of WO₃ nanocubes with peculiar electrochemical properties

A. K. H. Bashir • R. Morad • A. C. Nwanya • M. Akbari • J. Sackey • K. Kaviyarasu • I. G. Madiba • F. I. Ezema • M. Maaza

Received: 4 August 2020 / Accepted: 4 January 2021 / Published online: 29 January 2021 © The Author(s), under exclusive licence to Springer Nature B.V. part of Springer Nature 2021

Abstract A non-energy intense route was used for the synthesis of highly crystalline WO₃ nanocubes. The morphological studies confirmed the cuboidal shape of the nanocrystals. Raman spectrum result for the synthesized sample revealed that the vibrational modes correspond to those ones assigned to single phase stoichiometric WO₃. The band gap Eg was derived based on UV-Vis diffuse

This article is part of the topical collection: Nanotechnology Convergence in Africa

Guest Editors: Mamadou Diallo, Abdessattar Abdelkefi, and Bhekie Mamba

A. K. H. Bashir

Department of physics, Sudan University of Science and Technology, 11113 Khartoum, Sudan e-mail: abashiruwc@gmail.com

A. K. H. Bashir · R. Morad · A. C. Nwanya · M. Akbari · J. Sackey · K. Kaviyarasu · I. G. Madiba · F. I. Ezema · M. Maaza

UNESCO-UNISA Africa Chair in Nanosciences/Nanotechnology Laboratories, College of Graduate Studies, University of South Africa (UNISA), Muckleneuk ridge, PO Box 392, Pretoria, South Africa

M. Maaza

e-mail: Maaza@tlabs.ac.za

A. K. H. Bashir · R. Morad · A. C. Nwanya · M. Akbari · J. Sackey · K. Kaviyarasu · I. G. Madiba · F. I. Ezema () · M. Maaza Nanosciences African Network (NANOAFNET), iThemba LABS-National Research Foundation, 1 Old Faure Road, PO Box 722, Somerset West, Western Cape 7129, South Africa e-mail: fabian.ezema@unn.edu

reflectance result and found to be 2.58 eV, whereas the photoluminescence (PL) result confirmed the blue emission for the synthesized sample. The structural and electronic properties of the orthorhombic WO_3 were studied within the spin-polarized density functional theory (SDFT) using various functionals. Results indicated that the orthorhombic WO_3 is non-magnetic and has a direct band gap in the range of 2.15–3.75 eV which depends on the exchange-correlation functional used in the theory. The electrochemical studies showed that the nanocubes exhibited a peculiar electrochemical behaviour. In fact, the charge transfer resistances relatively enhanced which may results in decreasing the capacitance of the highly crystalline WO_3 nanocubes.

Keywords WO $_3$ ·Nanocubes·Hydrothermal synthesis·Raman spectrum·Blue emission·Electrochemical properties·Density functional theory

Introduction

Tungsten trioxide (WO_3) is a multifunctional oxide which has been used in a wide range of scientific applications such as electrochromism (Bucha et al. 2016), gas sensor (Stankova et al. 2006), photo-catalysis (Li et al. 2010) and electrochemistry (Nwanya et al. 2014). Although most of the transition metal oxides are commonly used in these applications, but the importance of WO_3 arises from the fact its growth equally in all these fields in addition to chromic properties. Hence, the synthesis and analysis of WO_3 in nano-scale has become



31 Page 2 of 11 J Nanopart Res (2021) 23: 31

increasingly required because it can improve the performance of this important functional metal oxide and offers remarkable properties that do not exist in its bulk form. In this nano-domain, increased surface-to-volume ratio of WO₃ particles provides more surface area for both chemical and physical interactions compared to their bulk counterpart.

WO₃ is an important n-type semiconductor with a wide band gap. The band gap of nano-scaled WO₃ is around 2.6 eV at ambient conditions (Wang et al. 2019), which is blue shifted. Such band gap facilitates the potential usage of nano-scaled WO₃ for various optical applications, especially in photocatalysis and chromism. On other hand, nano-scale can enhance the electrochemical performance of WO₃; this is due to the small distance over which the lithium ions will diffuse as well as the ion insertion and store are higher without causing degradation in the electrode (Christou et al. 2015). Nanomaterials with low dimension morphologies, i.e., 1D and/or 2D, can provide good physical and chemical properties. Since the properties of WO₃ are strongly dependent on structure, size and shape, controllable synthesis is required. Hence, several methods have been devoted for the synthesis of WO₃ nanoparticles such as template-assisted growth (Sadakane et al. 2008), anodization (Mozalev et al. 2008), thermal evaporation (Cao et al. 2009), chemical vapour deposition (Blackman and Parkin 2005), arc discharge (Ashkarran et al. 2008) and pulsed laser deposition (Lethy et al. 2008). Among these methods, hydrothermal method (Wang et al. 2019) has attracted great attention by scientists due to its advantages such as simplicity, low-cost, accuracy and low growth temperatures. However, using above methods, WO₃ with particular morphologies has been obtained including two-dimensional shapes such as nanoplates (Yang et al. 2012), nanocubes (Wang et al. 2019) and nanosheet (Azam et al. 2018).

Recently, two-dimensional nanomaterials have attracted a lot of attention due to their supreme advantages such as high surface energies and large light exposed surface area (Kumar et al. 2018). In this work, based on the advantages of two-dimensional nanomaterials, we have successfully synthesized WO₃ nanocubes using a facile hydrothermal route. The structure, morphology, optical and electrochemical properties were analysed for the highly crystalline WO₃ nanocubes. In addition, first-principle calculations based on density functional theory (DFT) (Kohn et al. 1996) was applied to study the structural and electronic properties of orthorhombic phase of WO₃. In this work, the

lattice constants and the band gap were theoretically obtained through the standard DFT/GGA calculations using PBE (Perdew et al. 1996), PW91 (Perdew et al. 1992), and BLYP (Becke 1988; Lee et al. 1988) functionals as well as two hybrid functionals including B3LYP (Becke 1993; Stephens et al. 1994; Heyd et al. 2003; Giannozzi et al. 2009) and HSE (Zheng et al. 2011). Theoretical results were compared with experimental data.

Experimental details: hydrothermal synthesis of WO₃ nanocubes (NCs)

The chemical reagents used in the synthesis procedure of the WO₃ NCs were of high purity (99.99%) and used without further purification. In all the synthesis steps and washing of the synthesis product, distilled water was used. Sodium tungstate dihydrate powder (Na₂WO₄.2H₂O) was used as a precursor for the synthesis of WO₃ NCs. In a typical synthesis process, 1 g of (Na₂WO4·2H₂O) was dissolved into 20 ml of distilled water in a glassy beaker and a HCl (8 mol/L) solution was added drop wise until the pH of the mixture was adjusted to be around 2. The mixture was kept under continuous stirring for 40 min at room temperature and ambient pressure to form a WO₃·H₂O (Wang et al. 2019). The hydrothermal synthesis was performed by transferring the mixture into a 40-mL Teflon-lined stainless steel autoclave at 200 °C for 24 h. Then, the product was let to cool down naturally at room temperature, and the precipitates were filtered and washed with distilled water and ethanol for several times before drying at 70 °C for 10 h. The hydrothermal synthesis of WO₃ could be simply described by the two following equations:

$$Na_2WO_4 + HCl + nH_2O \Rightarrow H_2WO_4 \cdot nH_2O + 2NaCl$$
 (1)

$$H_2WO_4 \cdot nH_2O + 2NaCl \Rightarrow^{200^0C} WO_3NCs \tag{2}$$

Based on the above chemical reactions described by Eqs. (1 and 2), one can realize that this synthesis method can be considered as one-step synthesis as well as non-extensive energy method. In addition, the accuracy in the formation of highly crystalline WO₃ nanocubes in a regular or uniform manner. All these advantages make this hydrothermal method useful and effective for synthesis nanoparticles compared to some other



conventional methods which may require high growth temperature.

Characterization techniques

To identify phase and crystallography of the sample, XRD analysis was performed using a Bruker AXS D8 Advance with radiation ($\lambda_{\text{Cuk}} = 1.5406 \text{ Å}$). A T64000 micro-Raman spectrometer (HORIBA Scientific, Jobin Yvon Technology) with a 532-nm laser wavelength and spectral acquisition time of 120 s was used for Raman spectrum measurement of the sample. UV-Vis reflectance spectrum was recorded for the sample using Cary 5000 UV-Vis-NIR spectrophotometer with double beam. The morphological characterization and elemental compositions of the sample were performed using Zeiss crossbeam 540 FEG SEM and high resolution transmission electron microscopy (Tecnai 720). Electrochemical studies were performed using an Autolab potentiostat equipped with NOVA 2.0 software.

Computational methods

The ab initio calculations based on the density functional theory (DFT) carried out with the Quantum Espresso (Kohn et al. 1996; Giannozzi et al. 2009) package using the plane-wave basis sets and the Norm-Conserving pseudopotentials. Different functionals including the generalized gradient approximation (GGA) PBE, PW91 and BLYP as well as two hybrid functionals including B3LYP (Becke 1993; Stephens et al. 1994) and HSE (Heyd et al. 2003) were implemented to study the structural and electronic properties of the orthorhombic WO₃. The percentage of exact Hartree-Fock (HF) exchange in B3LYP and HSE was 25%. A cut-off energy of 550 eV was used for the plane-wave basis set. The convergence threshold for the electronic structure was considered 10⁻⁶ Ry. A Monkhorst-Pack kpoint sampling of $2 \times 2 \times 2$ with a smearing with a Gaussian broadening of 0.01 was used for the structural optimization. For the density of state calculations, a more accurate k-mesh was used.

First, we fully optimized both the lattice parameters (the volume and shape) and the atomic coordinates until all the forces on each ion were less than 0.0005~eV/Å. Then, we calculated the band gap of the fully optimized structure.

It is clear that the structure and the size of WO_3 have an important effect on its properties, including the band gap. Therefore, in order to compare with the experiment, we adapted the lattice constants from the XRD analysis and just optimized the position of atoms inside the unit-cell using DFT with the PBE and BLYP functionals. Then, the band gap was computed for the relaxed atoms.

Results and discussion

Crystal structure

As a preliminary step for characterizing our hydrothermally synthesized WO₃ NCs, we had performed the Xray diffraction (XRD) measurement at room temperature (RT). It is evident from literature that nanostructured WO₃ has various crystal structures depending on synthesis process and/or annealing temperature. These crystal structures include monoclinic I (γ-WO₃), monoclinic II (ε -WO₃), orthorhombic (β -WO₃), tetragonal $(\alpha$ -WO₃) and cubic WO₃ (Zheng et al. 2011). However, it is clear from Fig. 1 that the XRD pattern of our sample indicates the presence of orthorhombic phase of WO₃, which is consistent with the (JCPDS file no. 71-2141). Accordingly, we carried out Rietveld refinement on the XRD data based on orthorhombic structure of WO₃ using TOPAS Academy software (Bashir et al. 2016). The space group setting used for the Rietveld refinement was Pnma (No.62). The solid red line in Fig. 1 represents the calculated data whereas the circular symbols with the cyan colour represent the experimental data. It can be seen from Rietveld refinement that the calculated XRD profile matches well with the experimental data

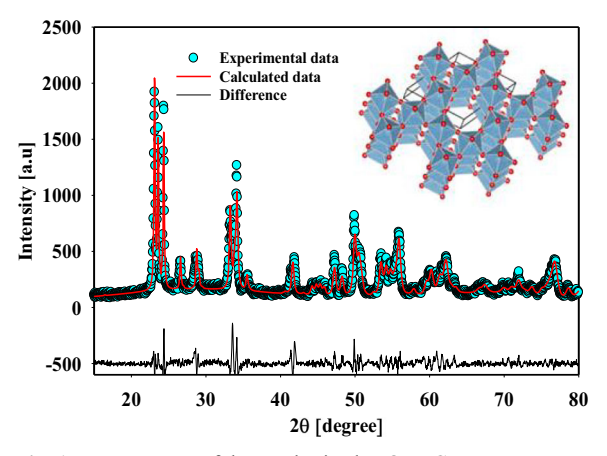
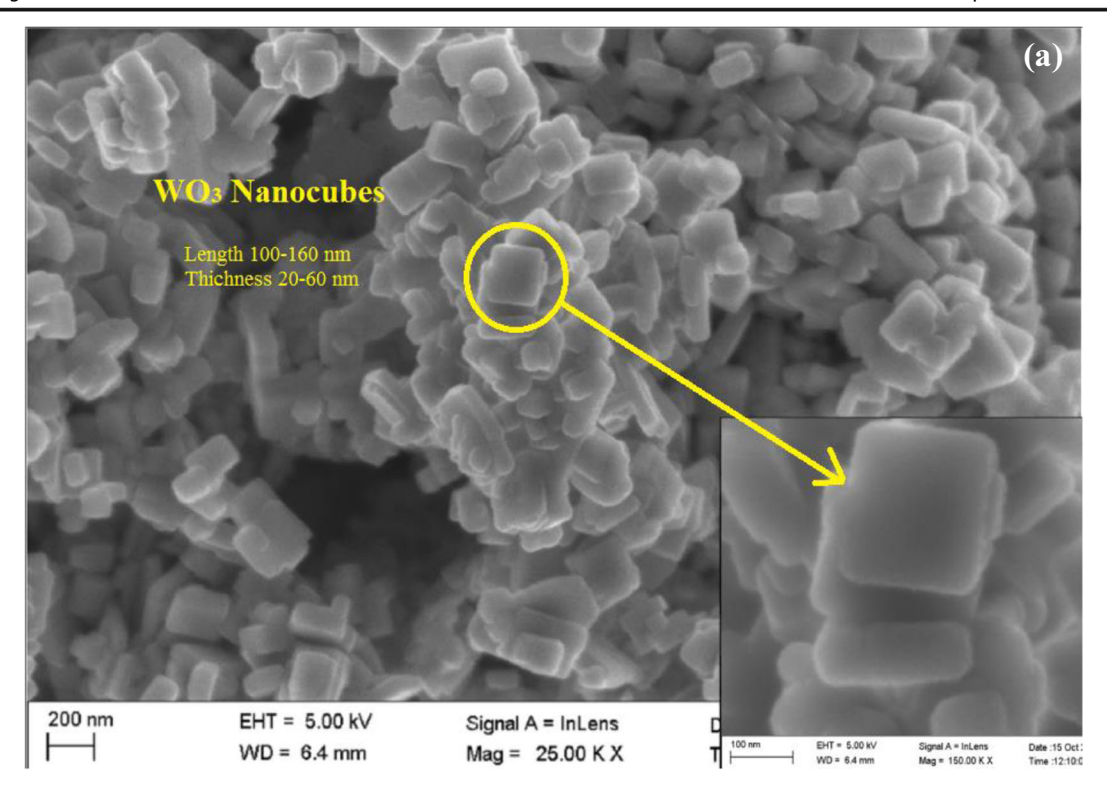


Fig. 1 XRD pattern of the synthesized WO₃ NCs



31 Page 4 of 11 J Nanopart Res (2021) 23: 31



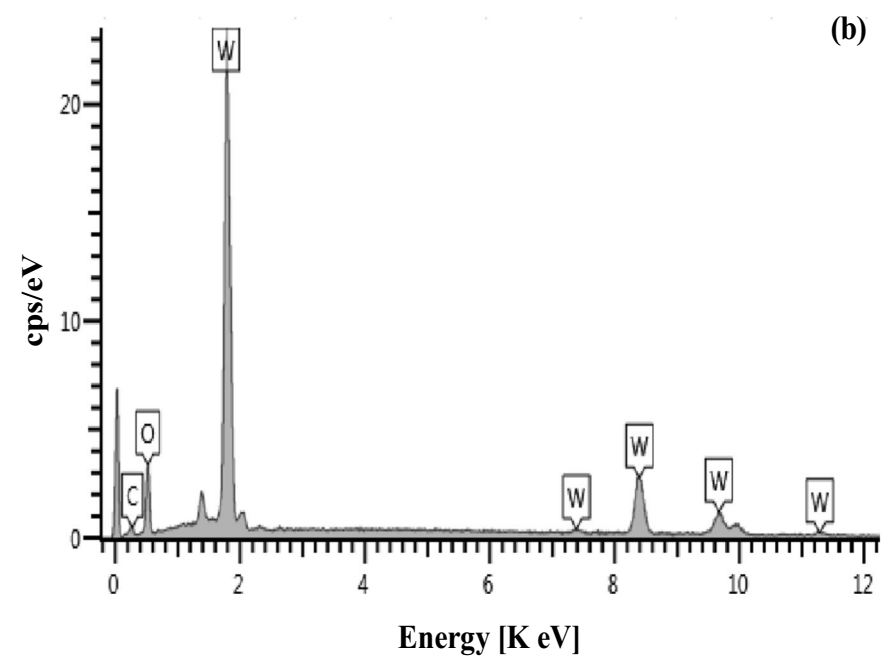


Fig. 2 a FESEM images of the synthesized WO₃ NCs. b EDS spectrum

across the entire range of measured angles which confirm the pure orthorhombic structure of WO₃ NCs. The crystal lattice constants a, b and c of the synthesized

 WO_3 NCs calculated from the Rietveld method were found to have the values 7.53889 Å, 7.69278 Å and 7.30659 Å, respectively. The inset of Fig. 1 displays the



crystal structure with atomic position of WO_3 , showing WO_6 octahedral and vacant sites. On the other hand, the sharp diffraction peaks of the XRD pattern reflect the good crystallizing of the synthesized sample. Moreover, no impurities' peaks have been observed in the XRD pattern.

Morphological analysis

The morphology of synthesized WO₃ NCs were studied using field-emission scanning electron microscopy (FESEM). Figure 2a displays the FESEM images of the synthesized sample in low and high magnifications. Both FESEM images show the nanocube structure of our sample of large dimension. The length and thickness of the nanocube were estimated using Image-J software and were found to be 100-160 nm and 20-60 nm, respectively. Also, electron dispersive X-rays spectroscopy EDS was used in order to check the elemental compositions of the synthesized sample and to confirm the absence of contamination during the hydrothermal synthesis. Figure 2b shows the EDS spectrum which revealed that the synthesized sample is only formed by W and O elements. The appearance of C element in the spectrum is due to the carbon-coated grid used during the measurement process.

Raman spectrum analysis

To further investigate the structure and vibrational modes of the synthesized WO₃ NCs, Raman spectrum was recorded. The measurement of the spectrum was performed at ambient conditions using laser source of 532 nm for the excitation the sample. Figure 3 shows

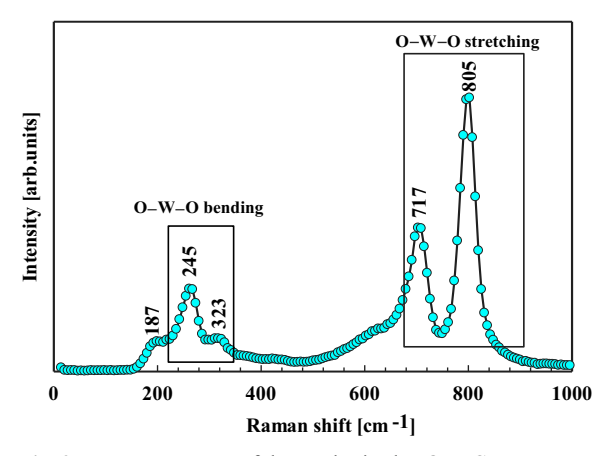


Fig. 3 Raman spectrum of the synthesized WO₃ NCs

Raman spectrum recorded for WO₃ NCs which revealed five Raman peaks. It was evident from literature that most of the vibrational modes of WO3 lattice are associated with stretching (γ) , the bending (α) , and the outof-plane wagging (γ) modes (Garcia-Sanchez et al. 2013). However, the five Raman peaks of the synthesized WO₃ NCs are located at 805 cm⁻¹, 717 cm⁻¹, 323 cm⁻¹, 245 cm⁻¹ and 187 cm⁻¹. The peaks located at 805 cm⁻¹ and 323 cm⁻¹ correspond to the stretching of O-W-O, while the peaks located at 717 cm⁻¹ and 245 cm⁻¹ are associated with the stretching of W–O, and the bending of O-W-O (Pecquenard et al. 1998; Habazaki et al. 2002), respectively. Finally, the peak below 200 cm⁻¹ which located at 187 cm⁻¹ is attributed to $(W_2O_2)_n$ chains (Pecquenard et al. 1998). It should be noted that the out-of-plane wagging $(\gamma)(O-W-O)$ modes at 670 cm⁻¹ is not presented in Raman spectrum of the synthesized WO₃ NCs, which can be attributed to high temperature (Garcia-Sanchez et al. 2013) that was used in hydrothermal synthesis process.

Optical properties

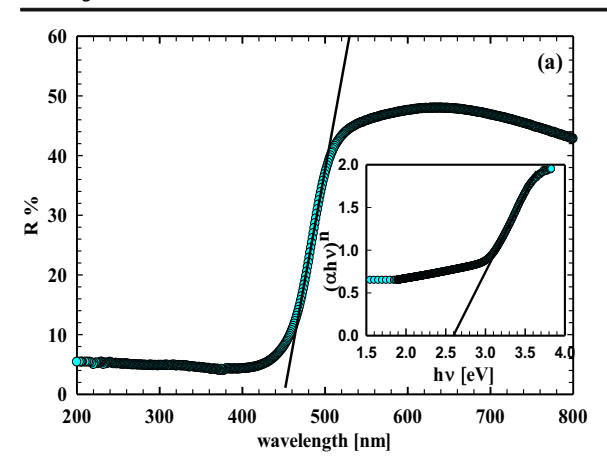
The optical properties such as band edge absorption, band gap and emission band peak of the synthesized WO₃ NCs were determined using UV-vis and PL techniques. Figure 4a exhibits the UV-vis diffuse reflectance spectrum of the synthesized WO₃ NCs measured at RT and in wavelengths range of 200–800 nm. It should be noted that a linear increase of the reflectance spectrum occurred in the wavelength between 450 and 500 nm before it tends to saturation. This gives strong evidence that the band edge absorption of WO₃ NCs is located around 450 nm, which is at visible light region. The band gap of the synthesized WO₃ NCs could be calculated based on UV-vis diffuse reflectance result using Tauc's equation (Ijeha et al. 2019) that given by:

$$(\alpha h \nu)^n = A(h \nu - E_g) \tag{3}$$

where hv is the photon energy, α is the optical absorption coefficient, A is a material-dependent constant and Eg is the energy band gap and n is an exponent which determines the type of the optical transition (Bashir et al. 2019), i.e. direct allowed, direct forbidden, indirect allowed and indirect forbidden transitions. The optical absorption coefficient of the materials is exponentially dependent on the photon energy. This is basically due to the electronic transitions occurring between localized



31 Page 6 of 11 J Nanopart Res (2021) 23: 31



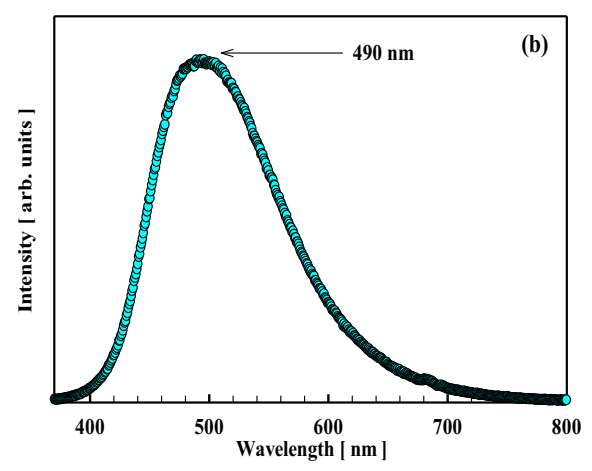


Fig. 4 a UV-vis diffuse reflectance spectrum of WO₃NCs. b PL spectrum

states which play an important role in determining the value of the energy band gap (Babu and Madhuri 2017). However, the exponent n takes the value of 1/2 of the indirect optical transition for WO₃ (Miyauchi 2008). Inset of Fig. 4a shows the plot of $(\alpha h \nu)^n$ against $(h \nu)$, which allows to calculate the energy gap by extrapolation of the straight-line graph at $(\alpha h \nu)^n = 0$. The band

Table 2 The experimental data vs the calculated DFT results at the level of GGA/PBE/plane wave of the theory

a (Å)	b (Å)	c (Å)	Band gap (eV)
7.53889	7.69278	7.30659	2.58
7.53889	7.69278	7.30659	2.52
7.53889	7.69278	7.30659	2.77
	7.53889 7.53889	7.53889 7.69278 7.53889 7.69278	a (Å) b (Å) c (Å) 7.53889 7.69278 7.30659 7.53889 7.69278 7.30659 7.53889 7.69278 7.30659

gap of the synthesized WO_3 NCs was found to be 2.57 eV which is plausible and in a good agreement with the reported previous studies (Wang et al. 2019; Miyauchi 2008).

PL spectrum exhibits only one peak centred at 490 nm which located at visible region and related to the Blue emission. The Blue emission in such materials often arises from the transitions between deep donor levels and the valence band (Bashir et al. 2020).

Structural and electronic properties from DFT

We studied orthorhombic WO₃ crystal structures with *Pnma* space group. The considered cell consists of 24 O and 8 W atoms. First, we fully optimized the cell with different functionals and the same norm-conserving pseudopotential from the Quantum Espresso pseudopotential library. The results of optimized lattice parameters, equilibrium volume and the band gap are listed in Table 1. Our results indicated that PW91 and HSE overestimate the equilibrium volume by 0.34% and 1.74%, respectively. While the PBE, BLYP, and B3LYP underestimate the equilibrium volume by 2.7%, 0.468 and 7.311%, respectively. Therefore, PW91 and BLYP predict the structural properties better.

The experimental band gap of WO₃ was reported in literature in the range of 2.5 to 3.2 eV (Granqvist 2000; Kharade et al. 2010; Gesheva et al. 2003; Gonzalez-Borrero et al. 2010). In our study, the hybrid functionals

Table 1 Calculated lattice parameters, equilibrium volume and band gap of the bulk orthorhombic WO3 by various DFT methods

Functional	a (Å)	b (Å)	c (Å)	Volume (ų/cell)	Band gap (eV)
Exp(Salje 1977)	7.24	7.57	7.75	53.9	
GGA/PW91	7.303	7.625	7.768	54.083	2.1547
GGA/PBE	7.142	7.602	7.719	52.393	2.6305
GGA/BLYP	7.162	7.681	7.800	53.647	2.8681
Hybrid/HSE	7.294	7.692	7.818	54.842	3.7591
Hybrid/B3LYP	7.025	7.470	7.615	49.958	5.2254



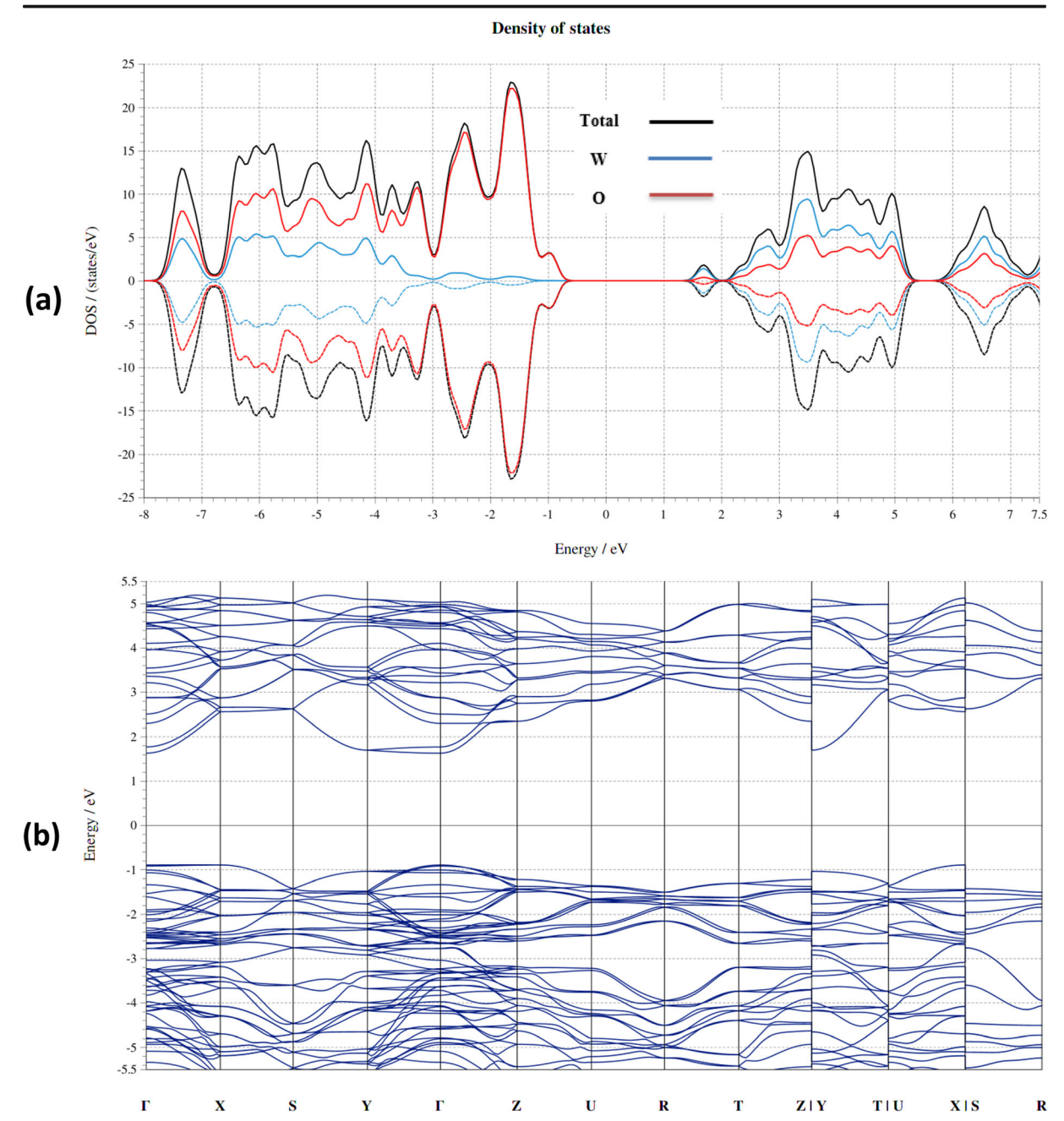


Fig. 5 a The electronic density of states (DOS) of the relaxed structure using SDFT with PBE functional. The black, red and blue curve shows the total, O, and W DOS. The upper and lower

panels indicate the spin up and the spin down DOS, respectively. ${\bf b}$ The corresponding band structure

with 25% of exact HF exchange overestimate the band gap, while the GGA/PW91 underestimates the band gap. The GGA/PBE and GGA/BLYP band gap is 2.63 and 2.86 eV, respectively which is in the range of reported experiments.

This work reported the synthesis of nano-scaled WO₃ NCs with the lattice parameters reported in Table 2. In order to compare the DFT calculations with the experiment, we adapted the lattice constants from the XRD analysis and just optimized the position of atoms inside



31 Page 8 of 11 J Nanopart Res (2021) 23: 31

the cell with the PBE and BLYP functionals which worked best in predicting both the structure and the band gap of bulk WO₃. The results are listed in Table 2. The band gap of PBE is 2.52 eV which is very close to our experimental value.

Figure 5 a and b show the PBE density of states (DOS) and the band structure, respectively. In this figure the Fermi energy sets to zero. The total magnetization of our spin polarized calculations of the WO₃ is zero; therefore, the density of states for spin up and down is exactly the same which indicates that the WO₃ has no magnetic moment. Also, one can see that the valence band mainly consists of the O electrons, while the valence electrons of W predominantly play a main role for the conduction band. The corresponding band structure shows that the band gap is direct at gamma point.

Electrochemical study

The cyclic voltammograms (CV) of the hydrothermally obtained WO_3 nanoparticles on glassy carbon electrode and the bare glassy carbon is as shown in Fig. 6a. The CV were obtained at 50 mV s⁻¹ in 3 M KOH in the potential

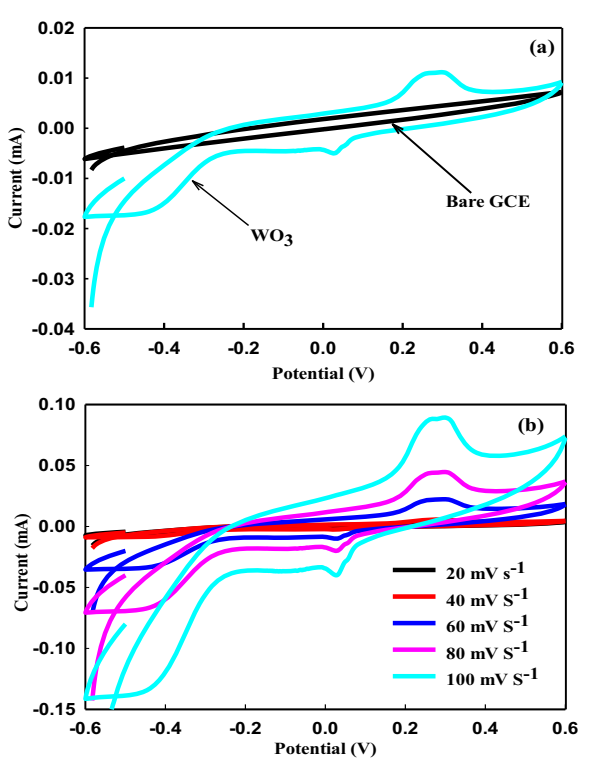
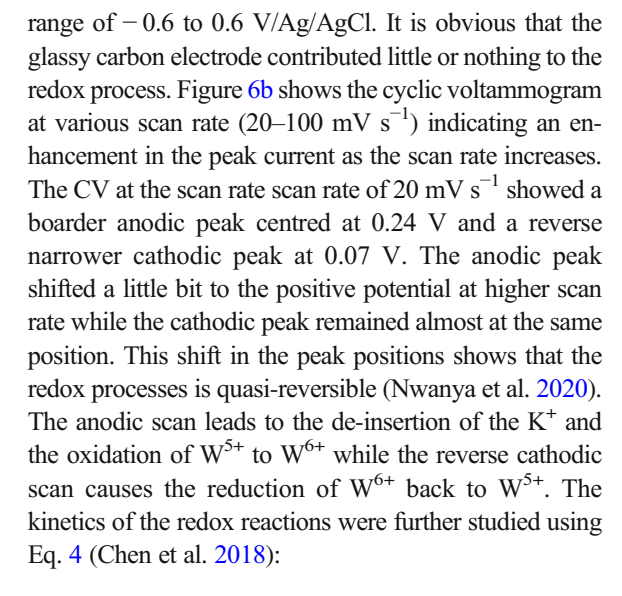


Fig. 6 Cyclic voltammetry in 3 M KOH of **a** bare GCE and GCE/WO₃ nanocomposites at 50 mV s⁻¹ and **b** GCE/WO₃ nanocomposites at different scans rates (20–100 mV s⁻¹)



$$I_{pa} = k_1 \nu + k_2 \nu^{1/2} \tag{4}$$

where I_{pa} is the anodic peak current, while k_1 and k_2 are respectively the capacitive and diffusion controlled contribution to the capacity. Our analysis shows the charge storage mechanism is dominated by diffusion-controlled reactions and a ratio of capacitive to diffusion-controlled capacity of 1:2 is obtained. The areal capacity was obtained from the cyclic voltammogram by integrating the absolute area under the curve using Eq. 5 (Nwanya et al. 2017):

$$Q_a = \frac{\int IdV}{A\nu} \tag{5}$$

where I, V, ν and A are respectively the current, potential window, scan rate and the area of the WO₃ on the GCE. Capacity value of 18.9 mC cm⁻² (18.9 mF cm⁻²; the potential window is 1 V) was obtained at a scan rate of 100 mV s⁻¹. Studies have shown that high crystalline WO₃ gives low capacities (Chen et al. 2018). Hence, the seemingly low capacity we obtained is most likely due to the high crystalline nature of the WO₃ NCs. However, the value of the areal capacitance obtained is a lot of improvement from 4 mF cm⁻² obtained by Nwanya et al. at a scan rate of 50 mV s⁻¹ (Nwanya et al. 2014). It is also comparable to 25 mF cm⁻² obtained by Zou et al. (Zou et al. 2014) for a composite of WO₃ and polyaniline at a scan rate of 5 mV s⁻¹.

The frequency response to the mechanism of the charge storage were further studied using electrochemical impedance spectroscopy (EIS) within the frequency



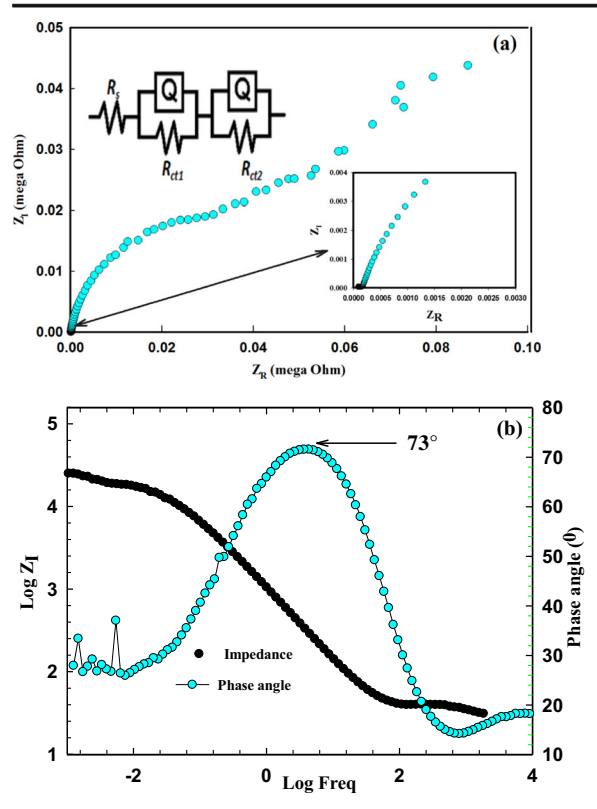


Fig. 7 a Nyquist plot. b Bode plot

range of 0.01 Hz to100 kHz at a voltage amplitude of 10 mV. The Nyquist plot (Fig. 7a) shows a distorted small semicircle (lower inset of Fig. 7a) at high frequency and terminates in a vertical line in the medium to low frequency region. The high frequency region is kinetics controlled and the distorted semicircle in this region gives the charge transfer resistances (Rct₁ and Rct₂) due to the migration of ions and electrons at the GCE/WO₃/electrolyte interfaces. The vertical line in the low frequency region is associated with the diffusion of ions to the electrode. The equivalent circuit (upper inset of Fig. 7a) and the values of the circuit elements (Table 3) were fitted using the *ZsimW in* software. The resistance

Table 3 Fitted values of circuit elements

Circuit element	Values
$\operatorname{Rs}\left(\Omega\right)$	131.20±4.15
Q1 (S-s)	$3.54\!\times\!10^{-5}\!\pm\!0.47\!\times\!10^{-5}$
Rct1 (MΩ)	0.14 ± 0.02
Q2 (S-s)	$5.40 \times 10^{-6} \pm 0.56 \times 10^{-6}$
Rct2 (k Ω)	223.70 ± 2.68

to the movement of ions in the electrolyte solution is depicted as the electrolyte resistance (R_s) while the inhomogeneity which occurs at GCE/WO₃/electrolyte interfaces is represented by the constant phase element (CPE or Q). The very large values of the charge transfer resistances may indicate low value of the capacitance of the high crystalline WO₃ NCs. The bode plot (Fig. 7b) showed a phase angle of 75° , which gives an indication that the charge storage mechanism is not governed by electric double layer capacitance.

Conclusion

In summary, the highly crystalline WO₃ nanocubes were synthesized via hydrothermal route at 200 °C. All characterization techniques used have confirmed the formation of WO₃ nanocubes. The analysis of the optical properties revealed that the band gap is blue shifted. The ab initio calculation in the spin-polarized DFT framework was performed to study the structural and electronic properties of bulk orthorhombic WO₃ using the plane wave QUANRUM-ESPRESSO package. Both standard DFT/GGA functionals and the hybrid functional were used in order to examine the best method to describe the bulk properties. It was found that the band gap of orthorhombic WO₃ in the GGA/PBE level of theory is 2.52 eV which is very close to the experimental value. In addition, all spin-polarized DFT calculations indicated that the orthorhombic WO3 is non-magnetic with direct band gap. Electrochemical result showed that the charge storage mechanism is not governed by electric double layer capacitance.

Acknowledgements Authors are grateful to the UNESCO-UNISA Africa Chair in Nanosciences and Nanotechnology(U2ACN2), The High Performance Computing (HPC), College of Graduate Studies, University of South Africa, the National Research Foundation of South Africa (NRF), iThemba LABS for the financial support and facilities. A.K.H Bashir thanks UNESCO-UNISA Africa Chair in Nanosciences and Nanotechnology (U2ACN2) for the (Post-Doctoral Fellowship programme under contract number: 90396898).

Compliance with ethical standards

Conflict of interest The authors declare that they have no conflict of interest.



31 Page 10 of 11 J Nanopart Res (2021) 23: 31

References

- Ashkarran AA, Irajizad A, Ahadian MM, Ardakani SAM (2008) Synthesis and photocatalytic activity of W₃ nanoparticles prepared by the arc discharge method in deionized water. Nanotechnology 19:195709–195716
- Azam A, Kim J, Park J, Novak TG, Tiwari AP, Song SH, Kim B, Jeon S (2018) Two dimensional WO₃ nanosheets chemically converted from layered WS2 for high performance electrochromic devices. Nano Lett 18:5646–5651
- Babu MB, Madhuri KV (2017) Structural, morphological and optical properties of electron beam evaporated WO₃ thin films. J Taibah Univ Sci 11:1232–1237
- Bashir AK, Tchokonte MBT, Strydom AM (2016) Electrical and thermal transport properties of RECu₄Au compounds, RE=Nd, Gd. J Magn Magn Mat 414:69–73
- Bashir AKH, Furqan CM, Bharuth-Ram K, Kaviyarasu K, Tchokonte MBT, Maaza M (2019) Structural, optical and Mössbauer investigation on the biosynthesized α-Fe₂O₃: study on different precursors. Phys E Low Dimens Syst Nanostruct 111:152–157
- Bashir AKH, Matinise N, Sackey J, Kaviyarasu K, Madiba IG, Kodseti L, Maaza M (2020) Investigation of electrochemical performance, optical and magnetic properties of NiFe₂O₄ nanoparticles prepared by a green chemistry method. Phys E Low Dimens Syst Nanostruct 119:114002
- Becke AD (1988) Exchange: density-functional exchange-energy approximation with correct asymptotic behavior. Phys Rev A 38(1988):3098 (subscription needed)
- Becke AD (1993) B3LYP: density-functional thermochemistry. III. The role of exact exchange. J Chem Phys 98:5648 (subscription needed)
- Blackman CS, Parkin IP (2005) Atmospheric pressure chemical vapor deposition of crystalline monoclinic WO_3 and WO_{3-x} thin films from reaction of WCl6 with O-containing solvents and their photochromic and electrochromic properties. Chem Mater 17:1583–1590
- Bucha VR, Chawlab AK, Rawalc SK (2016) Review on electrochromic property for WO₃ thin films using different deposition techniques Mater. Today Proceed 3:1429
- Cao B, Chen J, Tang X, Zhou W (2009) Growth of monoclinic WO₃ nanowire array for highly sensitive NO₂ detection. J Mater Chem 19:2323–2327
- Chen J, Wang H, Deng J, Xu C, Wang Y (2018) Low-crystalline tungsten trioxide anode with superior electrochemical performance for flexible solid-state asymmetry supercapacitor. J Mater Chem. A 6:8986–8991
- Christou K, Louloudakis D, Vernardou D, Katsarakis N, Koudoumas E (2015) Onepot syn thesis of WO₃ structures at 95°C using HCl. J Sol Gel Sci Technol 73:520–526
- Garcia-Sanchez RF, Ahmido T, Casimir D, Baliga S, Misra P (2013) Thermal effects associated with the Raman spectroscopy of WO₃ gas-sensor materials. J Phys Chem A 117: 13825–13831
- Gesheva K, Szekeres A, Ivanova T (2003) Photovoltaics and photoactive materials - properties, technology and applications. Sol Energy Mater Sol Cells 76:563–576
- Giannozzi P, Baroni S, Bonini N, Calandra M, Car R, Cavazzoni C, Corso AD (2009) Quantum espresso: a modular and open-

- source software project for quantum simulations of materials. J Phys Condens Matter 21(39):39550
- Gonzalez-Borrero PP, Sato F, Medina AN, Baesso ML, Bento AC, Baldissera G, Persson C, Niklasson GA, Granqvist CG, Ferreira da Silva A (2010) Optical band-gap determination of nanostructured WO₃ film. Appl Phys Lett 96:061909
- Granqvist CG (2000) Electrochromic tungsten oxide films: review of progress 1993-1998. Sol Energy Mater Sol Cells 60:201–262.
- Habazaki H, Hayashi Y, Konno H (2002) Characterization of electrodeposited WO3 films and its application to electrochemical wastewater treatment. Electrochim Acta 47:4181– 4188
- Heyd J, Scuseria GE, Ernzerhof M (2003) Hybrid functionals based on a screened Coulomb potential. J Chem Phys 118(18):8207–8215
- Ijeha RO, Nwany AC, Nkeleb AC, Khumalo Z, Madiba IG, Bashir AK, Osujib RU, Maaza M, Ezema F (2019) Magnetic and optical properties of electrodeposited nanospherical copper doped nickel oxide thin films. Phys E Low Dimens Syst Nanostruct 113:233–239
- Kharade RR, Mane SR, Mane RM, Patil PS, Bhosale PN (2010) Synthesis and characterization of chemically grown electrochromic tungsten oxide. J Sol-Gel Sci Technol 56:177
- Kohn W, Becke AD, Parr RG (1996) Density functional theory of electronic structure. J Phys Chem 100:12974–12980
- Kumar SK, Choudhary N, Jung Y, Thomas J (2018) Recent advances in two-. dimensional nanomaterials for supercapacitor electrode applications. ACS Energy Lett 3(2):482-495
- Lee C, Yang W, Parr RG (1988) Correlation: development of the Colle-Salvetti correlation-energy formula into a functional of the electron density. Phys Rev B 37:785 (subscription needed)
- Lethy KJ, Beena D, Mahadevan Pillai VP, Ganesan V (2008) Bandgap renormalization in titania modified nanostructured tungsten oxide thin films prepared by pulsed laser deposition technique for solar cell applications. J Appl Phys 104: 033515–033512
- Li L, Krissanasaeranee M, Pattinson SW, Stefik M, Wiesner U, Steiner U, Eder D (2010) Enhanced photocatalytic properties in well-ordered mesoporous WO₃. Chem Commun 46:7620– 7762
- Miyauchi M (2008) Photocatalysis and photoinduced hydrophilicity of WO₃ thin films with underlying Pt nanoparticles. Phys Chem Chem Phys 10:6258–6265
- Mozalev A, Khatko V, Bittencourt C, Hassel AW, Gorokh G, Llobet E, Correig X (2008) Nanostructured column like tungsten oxide film by anodizing Al/W/Ti layers on Si. Chem Mater 20:6482
- Nwanya AC, Jafta CJ, Ejikeme PM, Ugwuoke PE, Reddy MV, Osuji RU, Ozoemena KI, Ezema FI (2014) Electrochromic and electrochemical capacitive properties of tungsten oxide and its polyaniline nanocomposite films obtained by chemical bath deposition method. Electrochim Acta 128:21
- Nwanya AC, Obi D, Osuji RU, Bucher R, Maaza M, Ezema FI (2017) Simple chemical route for nanorod-like cobalt oxide films for electrochemical energy storage applications. J Solid State Electrochem 21:2567–2576
- Nwanya AC, Ndipingwi MM, Ikpo CO, Obodo RM, Nwanya SC, Botha S, Ezema FI, Iwuoha EI, Maaza M (2020) Zea mays



J Nanopart Res (2021) 23: 31 Page 11 of 11 **31**

lea silk extract mediated synthesis of nickel oxide nanoparticles as positive electrode material for asymmetric supercar battery. J Alloys Compd 822:153581.8–153581.15358225

- Pecquenard B, Lecacheaux H, Livage L, Julien C (1998) J Solid State Chem: 135, 159-168. Habazaki H, Hayashi Y, Konno H (2002). Electrochim Acta 47:4181–4188
- Perdew JP, Chevary JA, Vosko SH, Jackson KA, Pederson MR, Singh DJ, Fiolhais C (1992) Atoms, molecules, solids, and surfaces: applications of the generalized gradient approximation for exchange and correlation. Phys Rev B 46(11):6671
- Perdew JP, Burke K, Ernzerhof M (1996) Generalized gradient approximation made simple. Phys Rev Lett. 77(18):3865
- Sadakane M, Sasaki K, Kunioku H, Ohtani B, Ueda W, Abe R (2008) Preparation of nanostructured crystalline tungsten(VI) oxide and enhanced photocatalytic activity for decomposition of organic compounds under visible light irradiation. Chem Commun (48):6552–6556
- Salje E (1977) The orthorhombic phase of WO3. Acta Crystallogr B 33:574–577
- Stankova M, Vilanova X, Llobet E, Calderer J, Vinaixa M, Gracia I, Cane C, Correig X (2006) On-line monitoring of CO₂ quality using doped WO₃ thin film sensors. Thin Solid Films 500:302–308.554
- Stephens PJ, Devlin FJ, Chabalowski CF, Frisch MJ (1994) Ab initio calculation of vibrational absorption and circular

- dichroism spectra using density functional force fields. J Phys Chem 98:11623–11627
- Wang L, Hu H, Xu J, Zhu S, Ding A, Deng C (2019) WO3 nanocubes: hydrothermal synthesis, growth mechanism, and photocatalytic performance. J Mater Res 34(17):2955– 2963
- Yang J, Li W, Li J, Sun D, Chen Q (2012) Hydrothermal synthesis and photoelectrochemical properties of vertically aligned tungsten trioxide(hydrate) plate-like arrays fabricated directly on FTO substrates. J MaterChem 22:17744–17752
- Zheng H, Ou JZ, Strano MS, Kaner RB, Mitchell A, Kalantarzadeh K (2011) Nanostructured tungsten oxide properties, synthesis, and applications. Adv Funct Mater 21: 2175–2196
- Zou B, Gong S, Wang Y, Liu X (2014) Tungsten oxide and polyaniline composite fabricated by surfactant-templated electrodeposition and its use in supercapacitors. Journal of nanomaterials 2014:Article ID 813120

Publisher's note Springer Nature remains neutral with regard to jurisdictional claims in published maps and institutional affiliations.



Journal of Nanoparticle Research is a copyright of Springer, 2021. All Rights Reserved.